Evaluation of Heat Transfer Enhancement on Rotational Gas Turbine Blade Internal Cooling Channel With Dimpled Surface

Farah Nazifa Nourin
Department of Mechanical Engineering,
University of Wisconsin-Milwaukee,
115 East Reindl Way,
Glendale, WI 53212
e-mail: fnourin@uwm.edu

Brinn Leighton Blum
Department of Mechanical Engineering,
University of Wisconsin-Milwaukee,
115 East Reindl Way,
Glendale, WI 53212
e-mail: blblum@uwm.edu

Ryoichi S. Amano
Fellow ASME
Richard & Joanne Grigg Fellow Professor
Department of Mechanical Engineering,
University of Wisconsin-Milwaukee,
115 East Reindl Way,
Glendale, WI 53212
e-mail: amano@uwm.edu

The present investigation represents the rotational effect on gas turbine blade internal cooling with a uniform heat flux of 2000 W/m^2 at the bottom wall. The experiment was conducted with three different rpms, such as 300 rpm, 600 rpm, and 900 rpm, with Reynolds number (Re) ranging from 6000 to 50,000 with a two-pass cooling channel. The numerical investigation was conducted with the large eddy simulation (LES) technique to understand the rotational flow behavior of the cooling channel. Four distinct arrangements of dimpled cooling channel surfaces were considered with two different dimple shapes, i.e., partial spherical and leaf. It is found that the rotation effect, dimple arrangement, and design have significant influences on heat transfer. Results indicated that the partial spherical 1-row dimpled surface experienced the highest heat transfer coefficient and pressure drop. In contrast, the leaf-shaped dimpled cooling channel experienced the highest thermal efficiency. [DOI: 10.1115/1.4054288]

Keywords: gas turbine blade internal cooling, dimple, rotational cooling channel, heat transfer enhancement, large eddy simulation (LES), combustion of waste/fluidized bed, energy storage systems, power (co-) generation

1 Introduction

The gas turbine is one of the most widely used power generation equipment in today's world. It was first used back in 1939 for power generation [1]. With time, the demand for power increases, and the necessity for a more efficient turbine increases. There are five ways to improve the gas turbine efficiency: increase in turbine inlet temperature, use of regeneration, reheating and intercooling, and improvement in turbine metals. Among the possible opportunities to increase the efficiency, increasing the turbine inlet temperature is the most promising as it improves thermal efficiency. The higher inlet temperature demands for a metal surface which can withstand with it. Nowadays, several composite materials, such as nickel-based alloy, can withstand high temperatures. However, it is not good enough to resist at the 1600 °C surface temperature of a gas turbine blade. Therefore, efficient gas turbine internal cooling is mandatory. There are several cooling methods to cool the internal blade surface, such as smooth surface [2,3], dimple cooling [4,5], rib turbulator cooling [6,7], pin-fin cooling [8,9], and jet impingement cooling [10,11].

Researchers found that dimple cooling has outstanding heat transfer and energy management performance. Besides, it has a lower weight, low-pressure drop penalty, and simple fabrication. Figure 1 represents the flow mechanism responsible for heat transfer improvement by dimples. The flow gets separated at the entrance of dimples, and recirculation forms in the upstream half of the dimples, where the heat transfer is very low. The flow is reattached a little before exiting the dimples. The air experiences a flow circulation in the wide section of it. The flow mechanism is more or less the same for different dimple shapes. The slight change in flow pattern affects the heat transfer depending on the dimple shapes. The main factors for improving the heat transfer are flow separation, reattachment, impingement, and vortex roll generation.

A wide range of studies has been conducted with a dimpled surface for stationary cases based on dimple depth to diameter ratio, different shapes of dimples such as spherical, hemispherical, elliptical, and teardrop with other arrangements of dimple array [12–35]. The literature shows that the highest depth of dimpled surface experiences the highest heat transfers and pressure drop. The numerical model was primarily used Reynolds-averaged Navier–Stokes (RANS) models, such as k–ω, k–ω shear stress transport (SST), and k–ε turbulence model. The numerical study concluded that geometrical parameters such as the channel height ratio to the dimple diameter, the ratio of the dimple depth to diameter, and the angle of the major ellipse axis to flow direction caused a significant impact on the heat transfer boost.

The study of heat transfer augmentation in a rotational dimpled cooling channel is limited in the open literature. However, a few researchers investigated rotational cases. Zhou and Acharya [20] investigated the hemispherical depressions with rotation number 0.2 at Reynolds number 21,000. The leading and trailing surfaces were dimpled, and the other surfaces were smooth. The dimpled walls increase heat transfer over smooth surfaces, both stationary and rotational cases. The results also concluded that the maximum

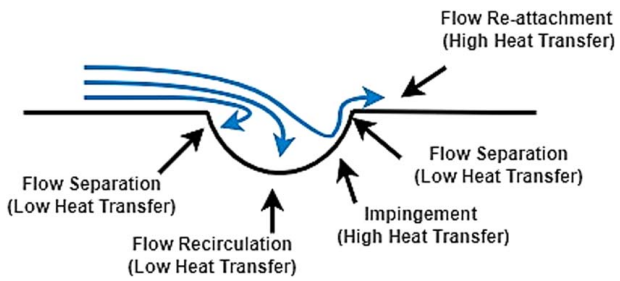

Fig. 1 Flow mechanism responsible for heat transfer improvement by dimples

Contributed by the Advanced Energy Systems Division of ASME for publication in the Journal of Energy Resources Technology. Manuscript received February 26, 2022; final manuscript received April 3, 2022; published online May 4, 2022. Editor: Hameed Metghalchi.

heat/mass transfer rates were obtained downstream of the dimples. The minimum rates were found along the row containing the dimples. Griffith et al. [36] and Kim et al. [37] revealed the reasons for enhanced heat transfer in rotational motion. The study was conducted for rotational numbers 0.04–0.3, varying the Reynolds number 5000–40,000. The two-channel orientation, i.e., 90 deg and 135 deg angled with the rotation plane, was considered. In a rotating dimpled channel, Coriolis vortex force significantly affects thermal behavior. The 90 deg angled channel experienced a heat transfer enhancement at the trailing surfaces of almost 100%. However, the leading surface showed little dependence on the rotation number. In the case of the 135 deg angled channel, the trailing outer surface showed an increase of more than 100% heat transfer. The trailing inner and leading exterior surfaces experienced approximately equal improvement in heat transfer, increasing by more than 50% from the stationary to the highest rotation number cases. Kim et al. [36] conducted an experimental study in a dimpled rotating test rig. They concluded that the heat transfer coefficient on the trailing surface is higher than that on the leading surface.

Amano et al. [38–42] studied various rotational speeds for a gas turbine blade internal cooling channel and reported the heat transfer and flow variations in a crossflow region depending on the rotating speed. The numerical study was conducted with different turbulence models such as k–ω, k–ε Reynolds-stress model (RSM), and large eddy simulation (LES) with rotation numbers ranging from −0.4 to 0.4 clockwise and counter-clockwise. The research team conducted the research with smooth and ribbed surfaces both computationally and experimentally up to 600 rpm.

The present experimental study was conducted with the highest rpm, i.e., 900 rpm, which corresponds with the Reynolds number ranging from 6000 to 50,000 for four different cases. Partial sphere and leaf dimpled surface were considered in this study, with a smooth surface cooling channel as a baseline case. The numerical study was conducted by implementing the large eddy simulation technique.

2 Experimental Methods

An experimental setup was built in the gas turbine lab of the University of Wisconsin-Milwaukee to run the rotational cases. The setup can run a maximum of 900 rpm. Figure 2 represents the cooling channel geometry. The inlet leg is 490 mm, and the outlet leg is 460 mm long with a hydraulic diameter of 40 mm. The setup was built using steel A −36 alloy. Dimples were designed with a 3D printer and glued to the bottom surface of the steel mold. The details of different channels can be observed in Table 1, and the geometries of those channels are shown in Fig. 3. A variable transformer was employed to apply a constant heat flux of 2000 W/m^2 to the bottom surface. The airflow was supplied with a blower, and a variable frequency drive (VFD) was used to control the airspeed. A set of wireless K- type thermocouples were used to record the temperature of the bottom surface. The wireless thermocouples send the signal to the computer with the help of an adapter. The locations of the thermocouples are included in Table 2. Figure 4 represents a block diagram of the experimental setup where the cooling channel was shown in the Z-direction for the ease of pictorial representation. In contrast, the channel was considered in the X-direction in both experimental and numerical studies. All the studied cases has been represented in Table 3.

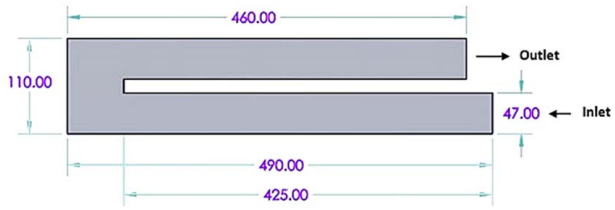

Fig. 2 Dimensions of the cooling channel (all dimensions are in mm) [36]

3 Physical Model and Boundary Conditions

The numerical solutions were set up to understand the flow behavior of the rotational cases with Re = 6000, 30,000, and 50,000 for the 900 rpm. The LES solution technique was considered. No-slip velocity condition was set to the walls. Turbulent velocity distribution was selected for the inlet, and a pressure outlet was set for the outlet. The inlet boundary condition was set as velocity inlet and segregated flow. To compare with the experimental results, the same heat flux, i.e., 2000 W/m^2 was applied to the bottom surface of the channels, and the rest of the wall was considered adiabatic.

The mesh independent study was conducted for 1.8, 2.5, 4.2, and 10 million cells for Case C. Figure 5 shows the surface average Nusselt number (Nu) for four different cells at Re = 30,000. The 2.5 and 4.2 million cells have the closer Nu number. The LES solution takes a substantial time to complete a solution. Thus, the 2.5 million cells were considered for all the cases. The physical time is 2 s with time-step 0.0001 s. Surface remesher and prism layers were considered. There was a total of 12 prism layers set to capture the near-wall behavior with 1.2 stretching of the cells. Figure 6 reveals the meshed scene for Case C at Re = 30,000.

An implicit unsteady solver was considered in these solutions, which resulted in a maximum convective Courant number (CCN) of 0.36 for a smooth surface and 0.54 partial spherical dimpled surface at the maximum Re number = 50,000 at 900 rpm. Figure 8 represents the Wall Y+ behavior of Case C. Wall distance, Y+, indicates the nondimensional distance from a wall. The maximum value of wall Y+, 0.91, was found in the bend section of the channel. In the bend section, airflow changes its flow direction and becomes more turbulent.

4 Data Reduction, Error, and Uncertainty Analysis

The convective heat transfer coefficient, h, was calculated with the constant heat flux, Q'' delivered through the variable transformer, surface and local air temperature were recorded from the thermocouple data. With the combination of hydraulic diameter, D_h and thermal conductivity, k, Nusselt number (Nu)

Table 1 Channel details

Channel name	Surface type	Number of dimples in leg 1	Number of dimples in leg 2	Dimple diameter (mm)	Dimple depth (mm)	Dimples depth to diameter ratio	Percentage of area occupied by dimples (%)
Case A	Smooth	N/A	N/A	N/A	N/A	N/A	N/A
Case B	Partial sphere	8 × 1	7 × 1	40	10	0.25	20.65
Case C	Partial sphere	8 × 2	7 × 2	20	10	0.50	10.30
Case D	Leaf	8 × 2	7 × 2	20	10	0.50	10.30

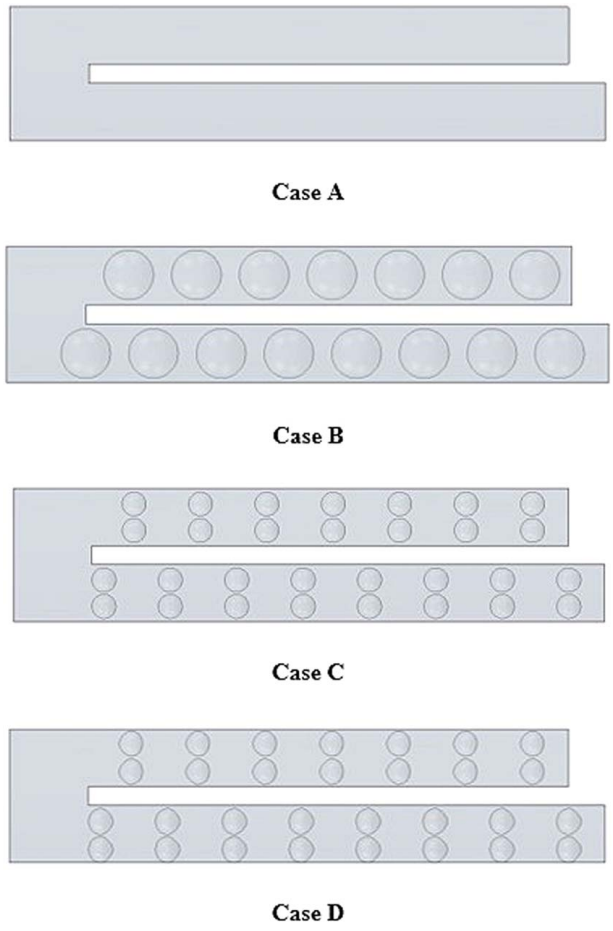

Fig. 3 Geometry of all the channels

was calculated [43]

$$h = \frac{Q''}{T_s - T_\infty} \tag{1}$$

$$\mathrm{Nu} = \frac{h \times D_h}{k} \tag{2}$$

Table 2 Thermocouple locations along the cooling channel

Thermocouple number	Thermocouple locations
1	210 mm from the inlet
2	300 mm from the inlet
3	360 mm from the inlet
4	410 mm from the inlet
5	450 mm from the inlet
6	480 mm from the inlet
7	Bend is the location at the center
8	350 mm from the outlet
9	200 mm from the outlet
10	100 mm from the outlet
11	70 mm from the outlet
12	40 mm from the outlet
13	10 mm from the outlet

The theoretical Nusselt number, Nu_o, for the turbulent flow, was calculated using the Dittus–Boelter equation [36]

$$\mathrm{Nu}_o = 0.023 \times \mathrm{Re}^{0.8} \times \mathrm{Pr}^{0.4} \tag{3}$$

The thermal efficiency was calculated to determine the optimized cooling channel with the optimum heat transfer and pressure drop. The friction factor, f, represents the pressure drop performance of the cooling channels. The Darcy friction factor of the flow across the cooling channel can be shown as follows [43]:

$$f = \frac{\Delta P}{(L/D_h)(1/2\rho u^2)} \tag{4}$$

Friction factors for all channels were normalized with the Blasius formula [36]. For $\mathrm{Re} < 10^5$, the Blasius formula for the friction factor is as follows:

$$f_o = 0.316\ \mathrm{Re}^{-0.25} \tag{5}$$

The thermal performance, η, is the function of the Nu number and friction factor, which leads to

$$\eta = \frac{\mathrm{Nu}/\mathrm{Nu}_o}{(f/f_o)^{1/3}} \tag{6}$$

The Reynolds number was evaluated using the air velocity supplied to the cooling channel. The standard properties of density, ρ, and dynamic viscosity (air), μ, were considered. The hydraulic

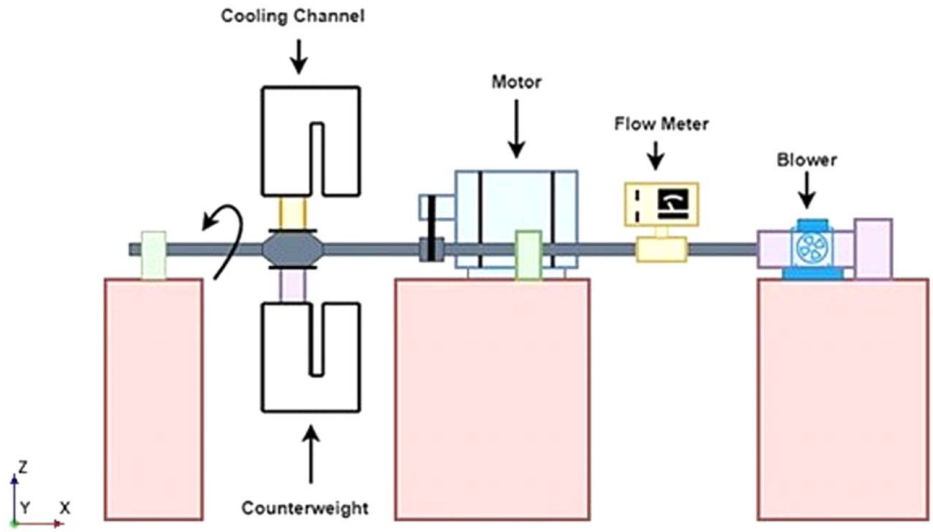

Fig. 4 Block diagram of the experimental setup [43]

Table 3 Summary of experimental cases

Cooling surface	rpm	Rotation number
Case A	300	0.36, 0.15, 0.07
	600	0.71, 0.30, 0.13
	900	1.07, 0.45, 0.20
Case B	300	0.36, 0.15, 0.07
	600	0.71, 0.30, 0.13
	900	1.07, 0.45, 0.20
Case C	300	0.36, 0.15, 0.07
	600	0.71, 0.30, 0.13
	900	1.07, 0.45, 0.20
Case D	300	0.36, 0.15, 0.07
	600	0.71, 0.30, 0.13
	900	1.07, 0.45, 0.20

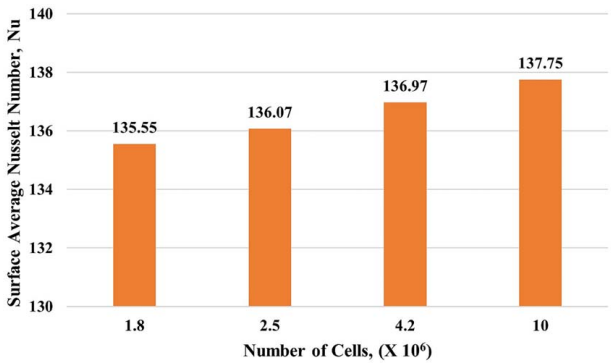

Fig. 5 Mesh independent study at Re = 30,000 for Case C

Fig. 6 Mesh scene with 2.5×10^6 number of cells

diameter, D_h, was counted as the characteristic length for the Reynolds number

$$\mathrm{Re} = \frac{\rho u D_h}{\mu} \tag{7}$$

The rotational speed was found from the controller of the rotation speed and leads to the calculation of the rotation number, which is

$$R_o = \frac{\Omega D_h}{u} \tag{8}$$

The computational model was validated with experimental results. Figure 9 represents the heat transfer along the leaf dimpled cooling channel. The scatter bars of Fig. 9 were generated using a 95% confidence interval. There is a slight difference between the experimental and computational results near the bend region. Near the bend region, the air gets more turbulent, which leads to an irregular airflow. Besides, the environment during the experiment was not ideal, while the perfect conditions were considered in the numerical study.

5 Results and Discussion

5.1 Heat Transfer Distribution. Due to rotational speeds, Coriolis force generates secondary forces inside the cooling

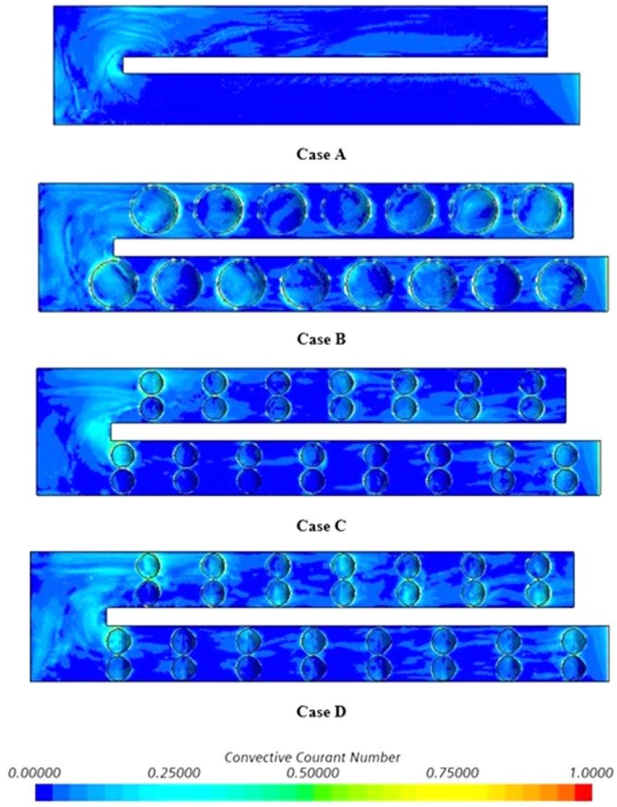

Fig. 7 Convective Courant number at $R_o = 0.20$

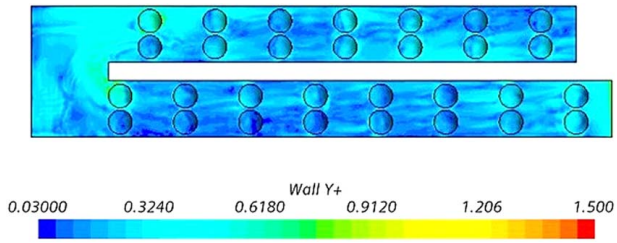

Fig. 8 Wall Y+ at $R_o = 0.20$

channel. It creates crossflow patterns. Density gradients cause the buoyancy forces, making the free convection heat transfer more significant. Figures 10–12 represent the heat transfer distribution along the smooth surface channel at the rotational speed of 300 rpm, 600 rpm, and 900 rpm. At the entrance of leg 1, the heat transfer is higher near the inlet. However, it decreases until the flow reaches the bend region. In the bend region, the U-turn induced secondary flow vortices which increases the heat transfer in this region.

The heat transfer distribution follows a similar trend along the dimpled surface channel (Figs. 13–21). Figures 13–15 represent the heat transfer along the dimpled cooling channel with a 1-row partial spherical dimple arrangement. For rotation numbers, $R_o =$ 0.07, 0.13, and 0.20, the heat transfer distribution in the bend region encounters a peak considering the other rotational number as at the highest air velocity, and the Coriolis force affects significantly. A similar trend is observed for Case C (Figs. 16–18). For Case D (Figs. 19–21), the heat transfer coefficient showed a higher peak right before and after the bend region as irregular airflow phenomena create more turbulence in this region. Additionally, the Coriolis and buoyancy force strongly affect the heat transfer here.

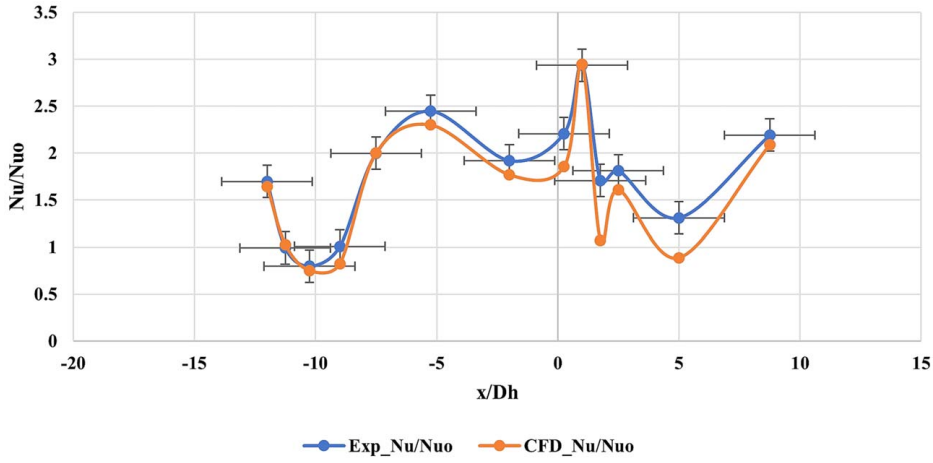

Fig. 9 Error analysis of experimental data at 95% confidence level (Case D at $R_o = 0.20$)

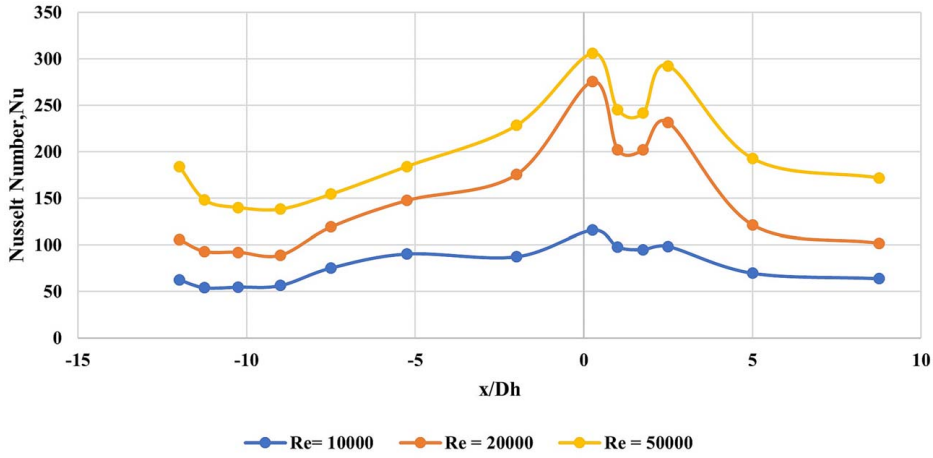

Fig. 10 Heat transfer distribution along the cooling channel of Case A at $R_o = 0.36$, 0.15, and 0.07

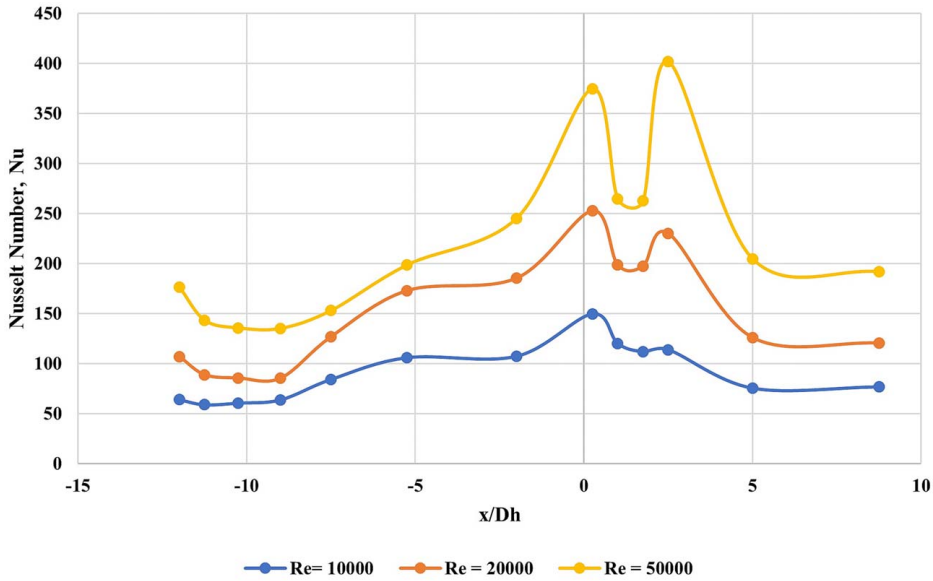

Fig. 11 Heat transfer distribution along the cooling channel of Case A at $R_o = 0.71$, 0.30, and 0.13

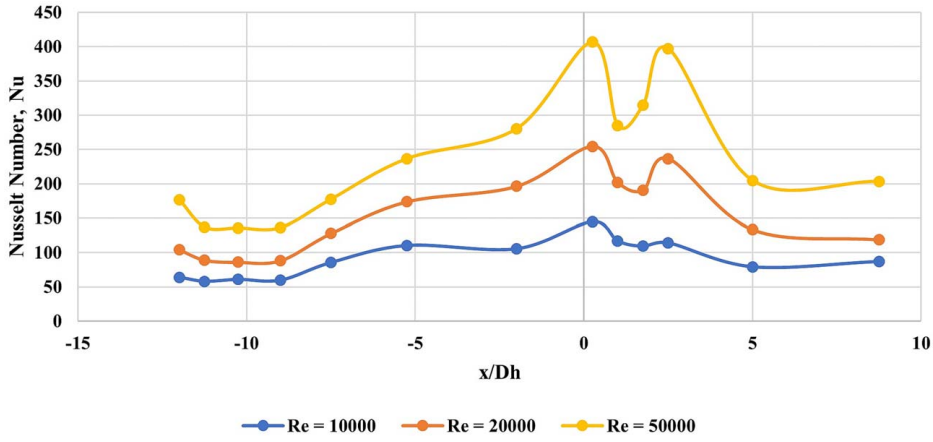

Fig. 12 Heat transfer distribution along the cooling channel of Case A at $R_o = 1.07$, 0.45, and 0.20

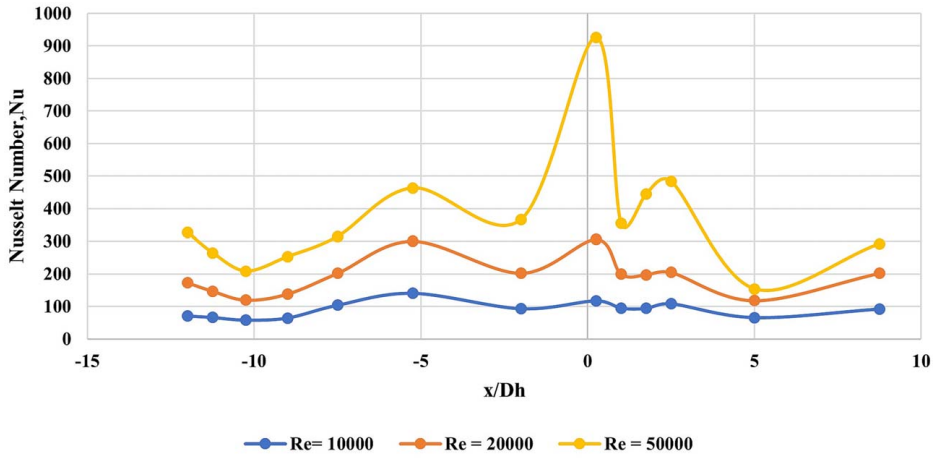

Fig. 13 Heat transfer distribution along the cooling channel of Case B at $R_o = 0.36$, 0.15, and 0.07

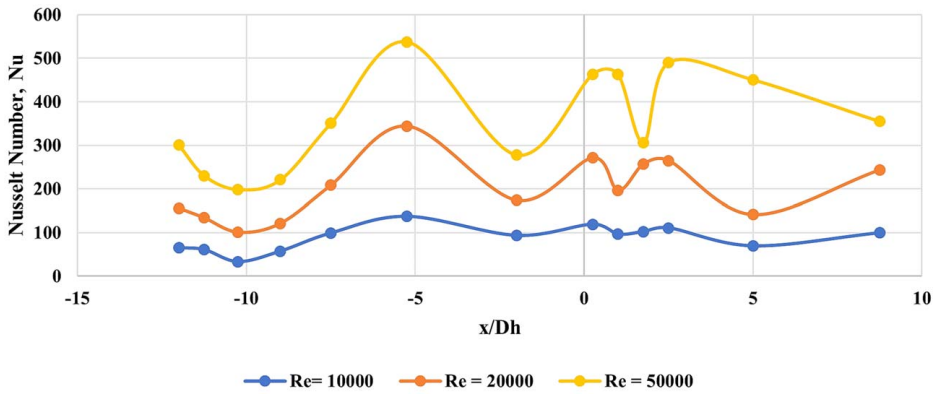

Fig. 14 Heat transfer distribution along the cooling channel of Case B at $R_o = 0.71$, 0.30, and 0.13

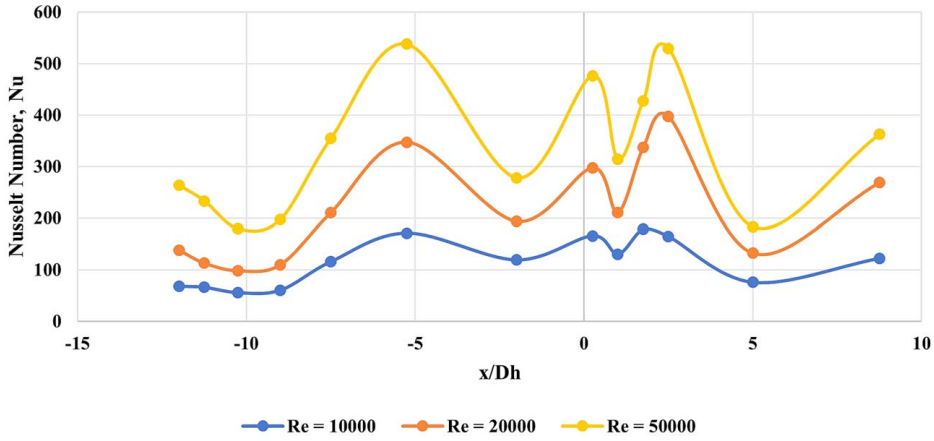

Fig. 15 Heat transfer distribution along the cooling channel of Case B at $R_o = 1.07$, 0.45, and 0.20

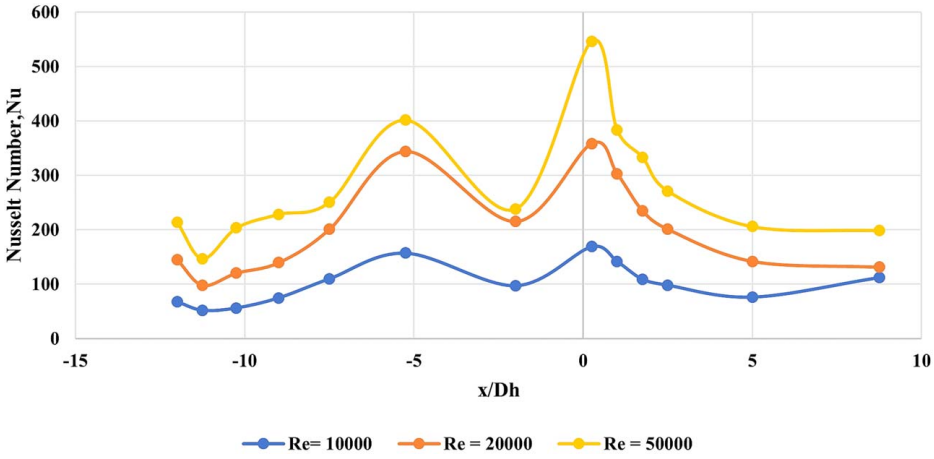

Fig. 16 Heat transfer distribution along the cooling channel of Case C at $R_o = 0.36$, 0.15, and 0.07

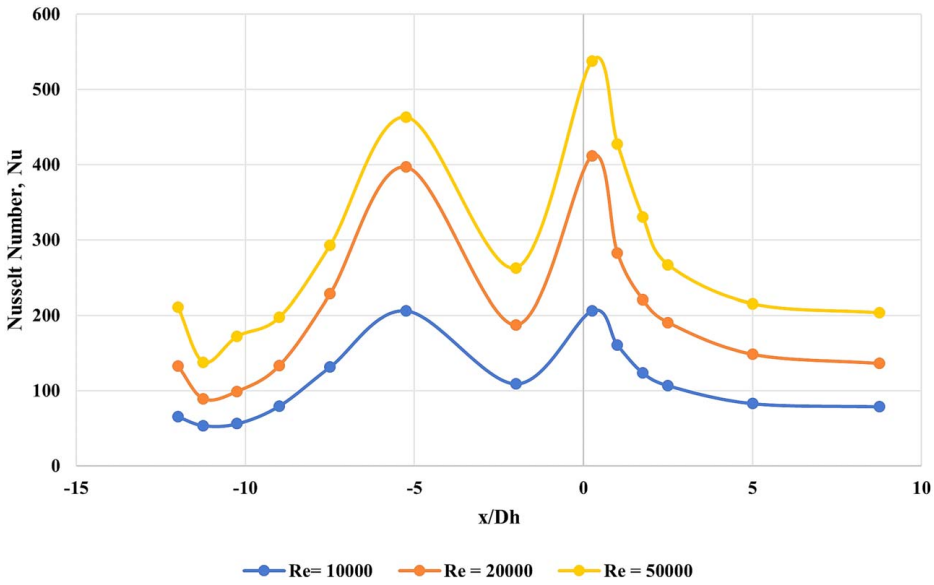

Fig. 17 Heat transfer distribution along the cooling channel of Case C at $R_o = 0.71$, 0.30, and 0.13

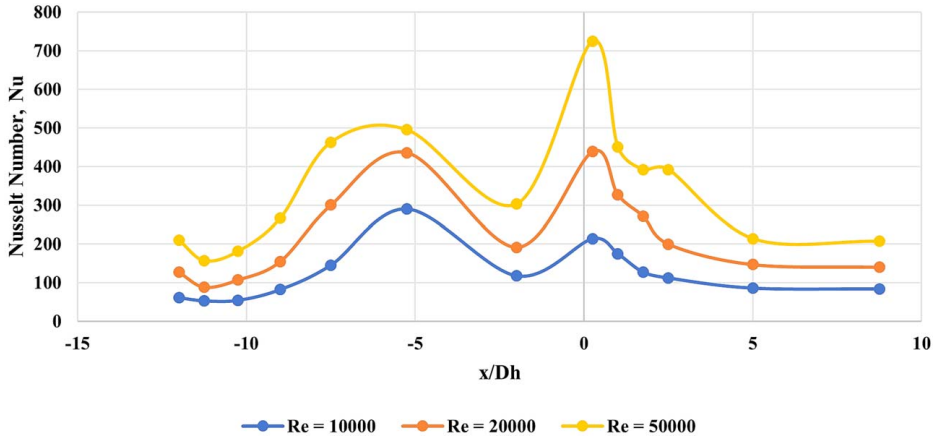

Fig. 18 Heat transfer distribution along the cooling channel of Case C at $R_o = 1.07$, 0.45, and 0.20

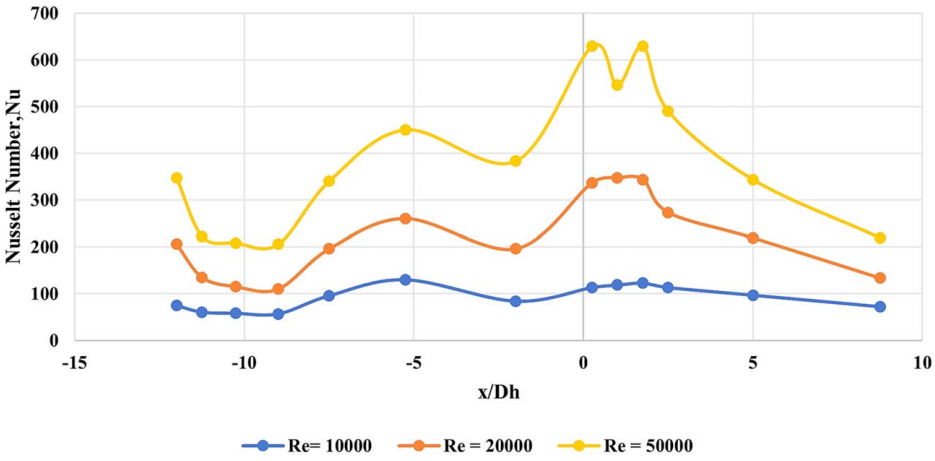

Fig. 19 Heat transfer distribution along the cooling channel of Case D at $R_o = 0.36$, 0.15, and 0.07

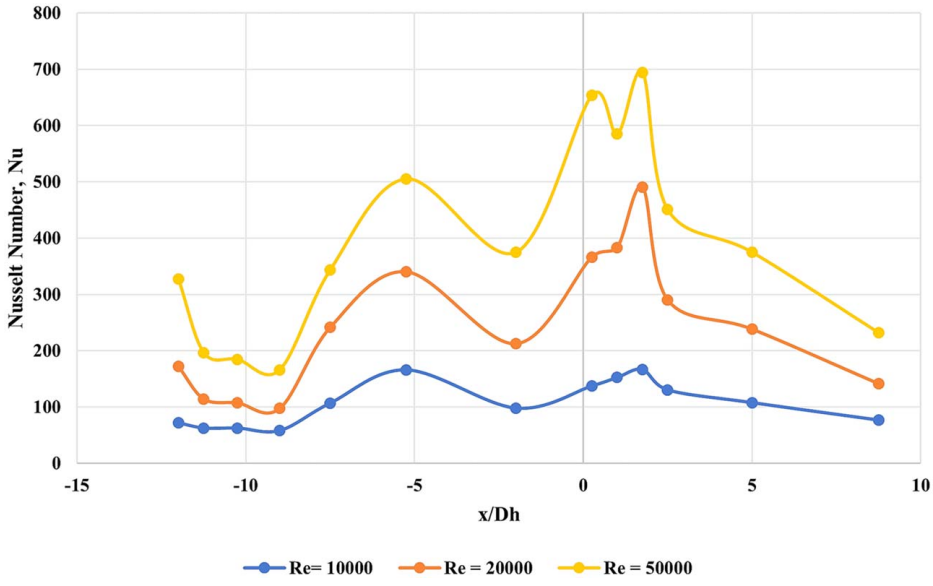

Fig. 20 Heat transfer distribution along the cooling channel of Case D at $R_o = 0.71$, 0.30, and 0.13

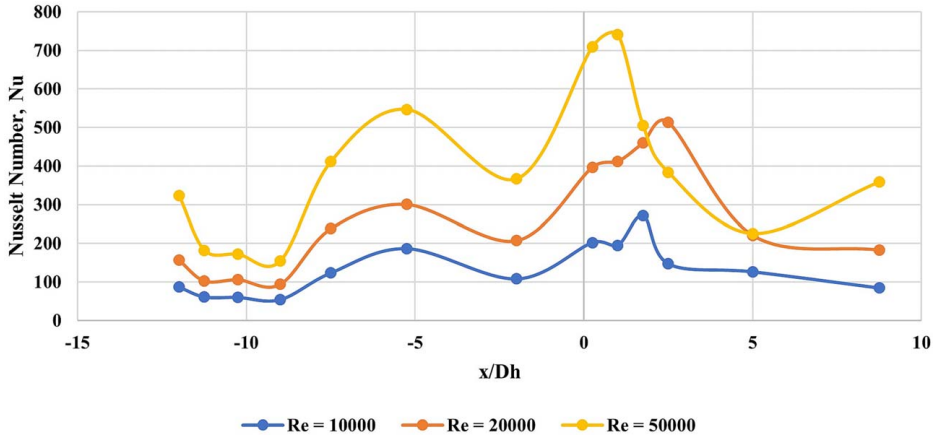

Fig. 21 Heat transfer distribution along the cooling channel of Case D at $R_o = 1.07$, 0.45, and 0.20

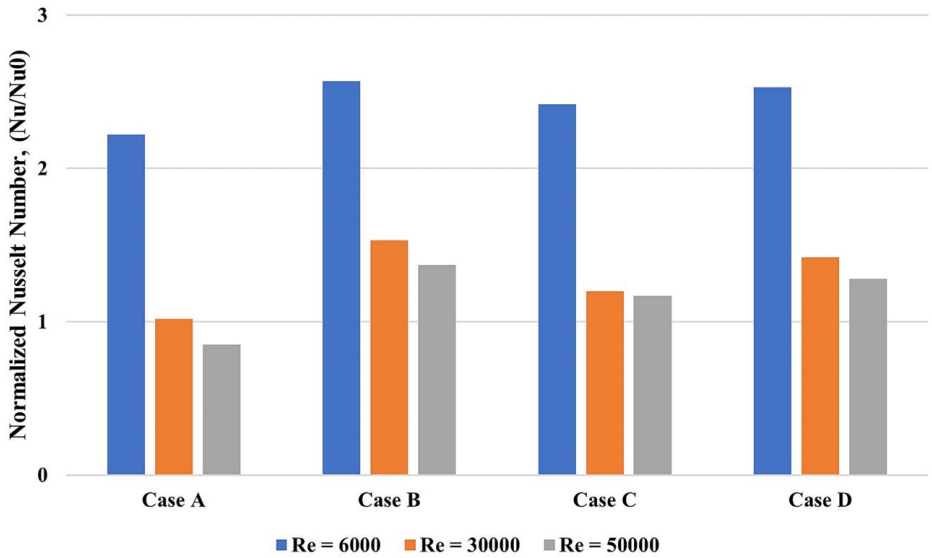

Fig. 22 Normalized Nusselt number for all the cases at $R_o = 1.07$, 0.45, and 0.20

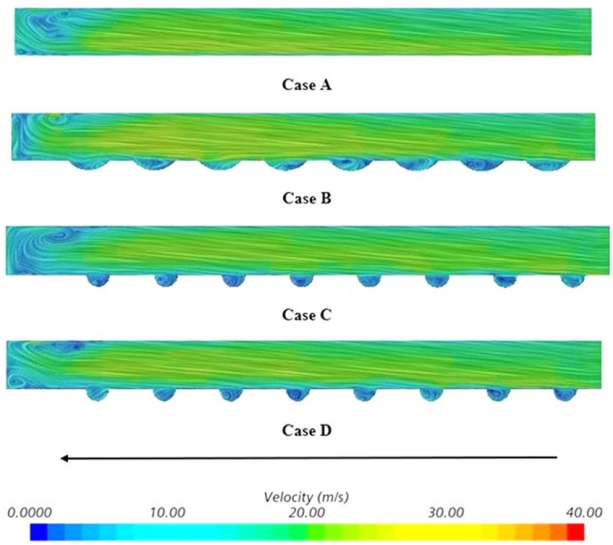

Fig. 23 Velocity distribution along leg 1 for different cases at Re = 50,000, rpm = 900, and $R_o = 0.20$

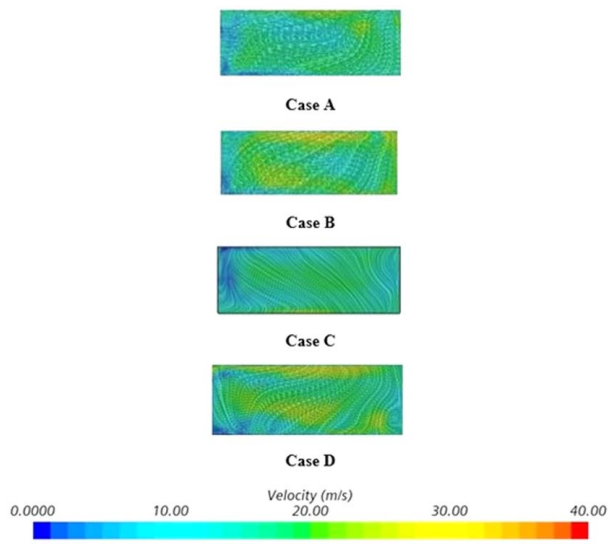

Fig. 24 Velocity distribution at bend for different cases at Re = 50,000, rpm = 900, and $R_o = 0.20$

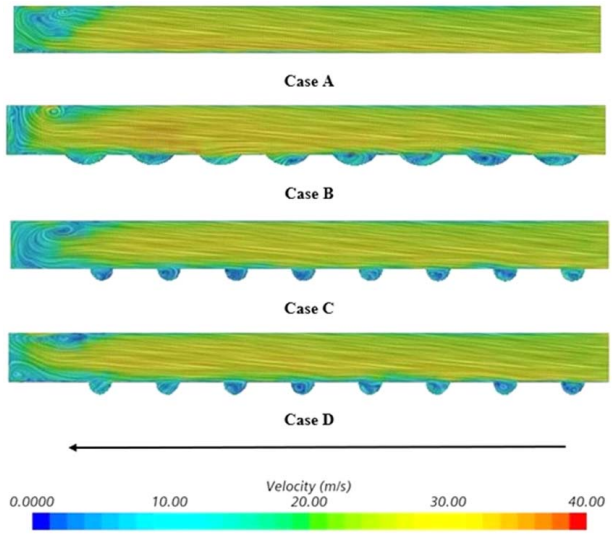

Fig. 25 Velocity distribution along leg 2 for different cases at Re = 50,000, rpm = 900, and $R_o = 0.20$

The heat transfer increases with the increase of Reynolds numbers regardless of the rotation speed (Fig. 22). Case B experiences the highest heat transfer distribution among the dimpled surface cases, i.e., Case C and Case D. The dimple depth is the highest for Case B, leading to the highest transfer. There is a significant change in normalized heat transfer from Re = 6,000 to Re = 30,000 due to the considerable airspeed change. Again, for Re = 30,000 and Re = 50,000, the heat transfer ratio shows a closer trend to each other.

5.2 Velocity Distribution Along the Channels. Figure 23 represents the velocity distribution at leg 1 for Re = 50,000 at 900 rpm. The flow pattern is different in the case of rotational cases. There is a strong effect of Coriolis and buoyancy forces in the rotational motions, which also increases the heat transfer in the case of the rotor and reduces the pressure drop. The entrance through before the bend, the flow pattern is regular. However, near the bend region, flow started getting irregular. The first vortex roll appears near the bend region for Case A. For Case B to Case D or dimpled cases, the first vortex appears at the first dimple, and near the bend section, the flow pattern is more irregular with huge turbulence. Figure 24 represents the velocity distribution

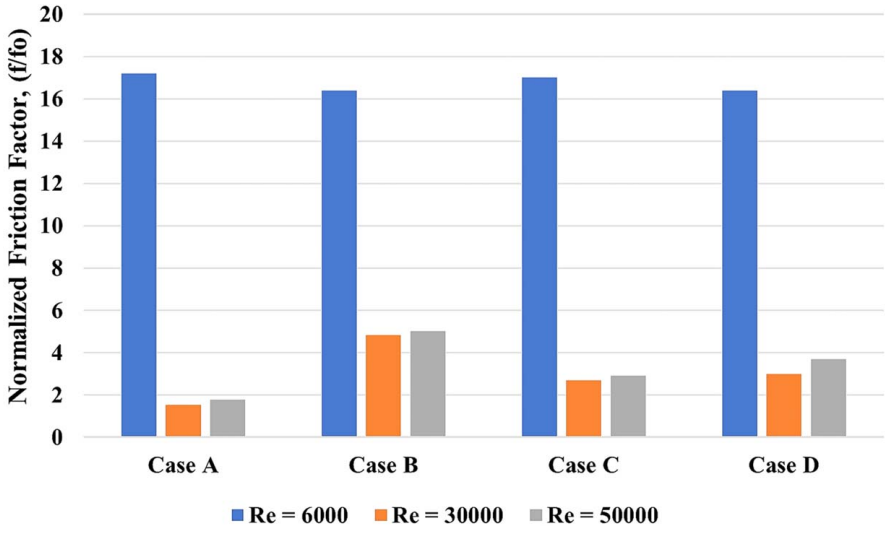

Fig. 26 Normalized friction factor for different channels at rpm = 900

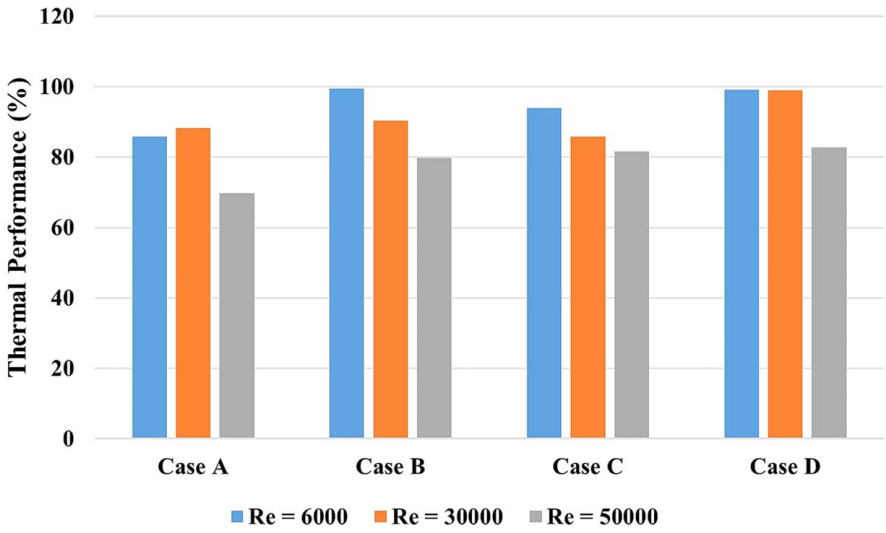

Fig. 27 Thermal performance for different channels at rpm = 900

at the bend region. Figure 25 represents the velocity pattern of leg 2. In leg 2, the direction of flow changes, and after the bend, it shows higher turbulence which carries around the mid-portion of leg 2. This phenomenon describes the higher heat transfer in the bend region and leg 2.

5.3 Thermal Performance. The rotational motion generates the buoyancy forces, which reduces the friction factor due to secondary flows. The pressure drop penalty can be observed in Fig. 26. Case B showed the highest pressure drop for all the Reynolds numbers due to the highest dimple depth. The smooth surface cooling channel has the lowest pressure drop penalty. However, the heat transfer is the lowest for a smooth surface cooling channel. The optimum heat transfer and pressure drop idea can be found in the thermal performance of the cooling channel (Fig. 27). The most efficient channel was found with a combination of leaf dimples with two arrays of dimples distribution along the cooling channel.

6 Conclusions

The experimental and numerical investigation was conducted for the rotational speed of 300 rpm, 600 rpm, and 900 rpm with Reynolds numbers ranging from 6000 to 50,000 with a smooth surface and dimpled surface cooling channel. The following observations can be made:

- The heat transfer increases with the increase of Reynolds number for all cases at all rotational speeds. Combining both increases the centrifugal and buoyancy forces, leading to the higher heat transfer in the cooling channel.
- The heat transfer is the highest for the highest dimple depth.
- Case D showed the optimum heat transfer and pressure loss due to the titled curve in its design.

Acknowledgment

The Department of Energy partially funded the experimental work (DOE EERE-PMC-DE-EE0000545). The computations are currently funded by NSF (NSF#2126229). The authors are profoundly grateful to the UWM high-performance computing center.

Conflict of Interest

There are no conflicts of interest.

Data Availability Statement

The authors attest that all data for this study are included in the paper.

Nomenclature

h = convective heat transfer coefficient (W/m^2 K)
k = thermal conductivity of air (W/m K)
u = velocity of air (m/s)
A = heater surface area (m^2)
F = friction factor ($f = \Delta P/((L/D_h)(\rho u^2/2))$)
H = thermal efficiency (%)
Q'' = convective heat flux (W/m^2)
f_o = smooth surface friction factor ($f_o = 0.316\mathrm{Re}^{-0.25}$)
D_h = hydraulic diameter (m)
R_o = rotation number ($R_o = \Omega D_h/u$)
T_s = surface temperature (K)
T_0 = local air temperature (K)
Nu = Nusselt number ($\mathrm{Nu} = hD_h/k$)
Nu_o = theoretical Nusselt number ($\mathrm{Nu}_o = 0.023\mathrm{Re}^{0.8}\mathrm{Pr}^{0.4}$)
Pr = Prandtl number
Re = Reynolds number

Greek Symbols

μ = dynamic viscosity of air (kg/m s)
ρ = density of air (kg/m^3)
Ω = rotational speed (rpm)

References

[1] The World's First Industrial Gas Turbine Set—GT NEUCHÂTEL, 2007, The American Society of Mechanical Engineers. Brosch_A4portrait_en_4.indd (asme.org). Accessed December 27, 2021.
[2] Saravani, M. S., DiPasquale, N. J., Abbas, A. I., and Amano, R. S., 2020, "Heat Transfer Evaluation for a Two-Pass Smooth Wall Channel: Stationary and Rotating Cases," ASME J. Energy Resour. Technol., **142**(6), p. 061305.
[3] Saravani, M. S., DiPasquale, N. J., Beyhaghi, S., and Amano, R. S., 2019, "Heat Transfer in Internal Cooling Channels of Gas Turbine Blades: Buoyancy and Density Ratio Effects," ASME J. Energy Resour. Technol., **141**(11), p. 112001.
[4] Nourin, F. N., and Amano, R. S., 2020, "Study on Heat Transfer Enhancement of Gas Turbine Blades," Int. J. Energy Clean Environ., **21**(2), pp. 91–106.
[5] Nourin, F. N., and Amano, R. S., 2022, "Experimental and Large Eddy Simulation Study for Visualizing Complex Flow Phenomena of Gas Turbine Internal Blade Cooling Channel With No Bend," ASME J. Energy Resour. Technol., **144**(6), p. 062104.
[6] Ashitaka, Y., 2010, "Heat/Mass Transfer Study on Ribbed Channel Flow in Gas Turbine Blade," Doctoral Dissertation, University of Wisconsin – Milwaukee, WI.
[7] Kumar, S., and Amano, R. S., 2012, November, "Numerical Simulation of Two-Pass Gas Turbine Blade Internal Cooling Channels With 90 Degree Varying Height Ribs," ASME International Mechanical Engineering Congress and Exposition, Houston, TX, Nov. 9–15, pp. 245–253.
[8] Jin, W., Jia, N., Wu, J., Lei, J. and Liu, L., 2019, June, "Numerical Study on Flow and Heat Transfer Characteristics of Pin-Fins With Different Shapes," Turbo Expo: Power for Land, Sea, and Air, Vol. 58646, American Society of Mechanical Engineers, Paper No. V05AT11A006.
[9] Effendy, M., Yao, Y., Yao, J., and Marchant, D. R., 2019, "Pin-Fin Shape and Orientation Effects on Wall Heat Transfer Predictions of Gas Turbine Blade," AIP Conference Proceedings, Surakarta, Indonesia, Dec. 12–13.
[10] Salem, A. R., Nourin, F. N., Abousabae, M., and Amano, R. S., 2021, "Experimental and Numerical Study of Jet Impingement Cooling for Improved Gas Turbine Blade Internal Cooling With In-Line and Staggered Nozzle Arrays," ASME J. Energy Resour. Technol., **143**(1), p. 012103.
[11] Nourin, F. N., Salem, A. R., and Amano, R. S., 2020, "Investigation of Jet Impingement Cooling for Gas Turbine Blade With In-Line and Staggered Nozzle Arrays," Int. J. Energy Clean Environ., **21**(2), pp. 169–182.
[12] Rashidi, S., Hormozi, F., Sundén, B., and Mahian, O., 2019, "Energy Saving in Thermal Energy Systems Using Dimpled Surface Technology—A Review on Mechanisms and Applications," Appl. Energy, **250**, pp. 1491–1547.
[13] Choi, E. Y., Choi, Y. D., and Kwak, J. S., 2013, "Effect of Dimple Configuration on Heat Transfer Coefficient in a Rib-Dimpled Channel," J. Thermophys. Heat Transfer, **27**(4), pp. 653–659.
[14] Chyu, M. K., Yu, Y., Ding, H., Downs, J. P. and Soechting, F. O., 1997, June, "Concavity Enhanced Heat Transfer in an Internal Cooling Passage," Turbo Expo: Power for Land, Sea, and Air, Vol. 78705, American Society of Mechanical Engineers, Paper No. V003T09A080.
[15] Moon, H. K., O'connell, T., and Glezer, B., 2000, "Channel Height Effect on Heat Transfer and Friction in a Dimpled Passage," ASME J. Eng. Gas Turbines Power, **122**(2), pp. 307–313.
[16] Mahmood, G. I., Hill, M. L., Nelson, D. L., Ligrani, P. M., Moon, H. K., and Glezer, B., 2001, "Local Heat Transfer and Flow Structure on and Above a Dimpled Surface in a Channel," ASME J. Turbomach., **123**(1), pp. 115–123.
[17] Xie, G., and Sundén, B., 2010, "Numerical Predictions of Augmented Heat Transfer of an Internal Blade Tip-Wall by Hemispherical Dimples," Int. J. Heat Mass Transfer, **53**(25–26), pp. 5639–5650.
[18] Rao, Y., Feng, Y., Li, B., and Weigand, B., 2015, "Experimental and Numerical Study of Heat Transfer and Flow Friction in Channels With Dimples of Different Shapes," ASME J. Heat Transfer-Trans. ASME, **137**(3), p. 031901.
[19] Nishida, S., Murata, A., Saito, H., and Iwamoto, K., 2009, "Measurement of Heat and Fluid Flow on Surface With Teardrop-Shaped Dimples," Proceedings of the Asian Congress on Gas Turbines, 2009-8, Tokyo, Japan, Aug. 24–26, pp. 1–4.
[20] Zhou, F., and Acharya, S., 2001, "Mass/Heat Transfer in Dimpled Two-Pass Coolant Passages With Rotation," Ann. N. Y. Acad. Sci., **934**(1), pp. 424–431.
[21] Galeana, D., and Beyene, A., 2021, "Gas Turbine Blade Heat Transfer and Internal Swirl Cooling Flow Experimental Study Using Liquid Crystals and Three-Dimensional Stereo-Particle Imaging Velocimetry," ASME J. Energy Resour. Technol., **143**(10), p. 102106.
[22] Kumar, S., and Amano, R. S., 2021, "An Investigation in the Numerical Approach to Solve the Heat Transfer Phenomenon in Gas Turbine," ASME J. Energy Resour. Technol., **143**(8), p. 080805.
[23] Nourin, F. N., and Amano, R. S., 2021, "Review of Gas Turbine Internal Cooling Improvement Technology," ASME J. Energy Resour. Technol., **143**(8), p. 080801.

[24] Amano, R. S., and Sunden, B., 2014, *Impingement Jet Cooling in Gas Turbines*, WIT Press, Boston, MA.
[25] Amano, R. S., Keenan, M., and Ou, S., 2014, *Impingement Jet Cooling in Gas Turbines*, WIT Press, Boston, MA, pp. 33–62.
[26] Amano, R. S., Sunden, B., and Brebbia, CA, 2008, *Advanced Computational Methods and Experiments in Heat Transfer X*, WIT Press, Southampton, UK, pp. 149–157.
[27] Amano, R. S., 2002, "Heat Transfer Predictions of Stator/Rotor Blades and Rotating Disk," *Heat Transfer in Gas Turbine Systems*, WIT Press, Southampton, UK, pp. 227–261.
[28] Forghan, F., Askari, O., Narusawa, U., and Metghalchi, H., 2016, "Cooling of Turbine Blade Surface With Expanded Exit Holes: Computational Suction-Side Analysis," ASME J. Energy Resour. Technol., **138**(5), p. 051602.
[29] Amano, R. S., 1995, "Turbulence Heat Transfer Characteristics in a Gas Turbine Stator-Rotor Stage," *Turbulence, Heat and Mass Transfer 1*, K. Hanjalic, and J. C. F. Pereira, eds., Begell House, Inc., Danbury, CT, pp. 459–465.
[30] Amano, R. S., 1996, "Turbulence Heat Transfer Characteristics in a Gas Turbine Stator-Rotor Stage," *Turbulence, Heat and Mass Transfer 1*, K. Hanjalic, and J. C. F. Pereira, eds., Begell House, Inc., Danbury, CT, pp. 459–465.
[31] Amano, R. S., Wang, K. D., and Pavelic, V., 1994, "A Study of Rotor Cavities and Heat Transfer in a Cooling Process in a Gas Turbine," ASME J. Turbomach., **116**(2), pp. 333–338.
[32] Amano, R. S., 2019, "Study on Heat Transfer of a Rotational Turbine Blade System," International Gas Turbine Congress, Tokyo, IGTC-2019-008, Toranomon, Minato-ku, Tokyo, Japan, Nov. 17–22.
[33] Dong, P., and Amano, R. S., 2017, "High-Pressure Gas Turbine Vane Turbulent Flows and Heat Transfer Predicted By RANS/LES/DES," GT2017-630322017 ASME Turbo & Expo, Charlotte, NC, June 26–30, p. V05BT22A001.
[34] Amano, R. S., and Kumar, S., 2016, "Gas Turbine Blade Cooling Passage With V and Broken V-Shaped Ribs," 11-2 Numerical Internal Cooling: Ribs, Pin Fins, and Pedestals—I, Proceedings of ASME Turbo Expo, Seoul, South Korea, June 13–17, p. V05BT11A001.
[35] Guntur, K. S., Kumar, S., and Amano, R. S., 2012, "Experimental and Numerical Evaluation of Geometric Modifications in Gas Turbine Blade Cooling Channel," 2012 50th AIAA Aerospace Sciences Meeting Including the New Horizons Forum and Aerospace Exposition, Jan. 9–12.
[36] Griffith, T. S., Al-Hadhrami, L., and Han, J. C., 2002, "Heat Transfer in Rotating Rectangular Cooling Channels (AR= 4) With Dimples," Turbo Expo: Power for Land, Sea, and Air, Amsterdam, Netherlands, June 3–6.
[37] Kim, S., Choi, E. Y., and Kwak, J. S., 2012, "Effect of Channel Orientation on the Heat Transfer Coefficient in the Smooth and Dimpled Rotating Rectangular Channels," ASME J. Heat Transfer-Trans. ASME, **134**(6), p. 064504.
[38] S. Saravani, M., and Amano, R. S., 2019, "Heat Transfer Enhancement in Stationary and Rotating Internal Cooling Channels Using Angled Ribs," AIAA SciTech, AIAA-2019-1275, San Diego, CA, Jan. 7–11, p. 1275.
[39] Amano, R. S., Martinez-Lucci, J. O., Guntur, K., and Song, B., 2012, "Numerical Study of the Thermal Development in a Rotating Cooling Passage," Heat Mass Transfer, **48**(6), pp. 1011–1022.
[40] Amano, R. S., and Song, B., 2005, "Simulation of Turbulent Flow in a Duct With and Without Rotation—Cooling Passage of Gas Turbine Blades," *Modeling and Simulation of Turbulent Heat Transfer*, WIT Press, Southampton, UK, pp. 315–348.
[41] Lucci, J. M., Guntur, K. S., and Amano, R., 2008, "Study of Flow and Thermal Development in a Rotating Cooling Passage," 46th AIAA Aerospace Sciences Meeting and Exhibit, AIAA-2008-1172, Reno, NV, Jan. 7–10.
[42] Song, B., and Amano, R. S., 2001, "On Turbulent Secondary Flows and Heat Transfer," ASME IGTI Turbo & Expo, 2001-GT-0188, Atlanta, GA, June 4–7.
[43] Nourin, F. N., and Amano, R. S., 2022, "Experimental Study on Flow Behavior and Heat Transfer Enhancement With Distinct Dimpled Gas Turbine Blade Internal Cooling Channel," ASME J. Energy Resour. Technol., **144**(7), p. 072101.